Fukata et al., http://www.jcb.org/cgi/content/full/jcb.201302071/DC1

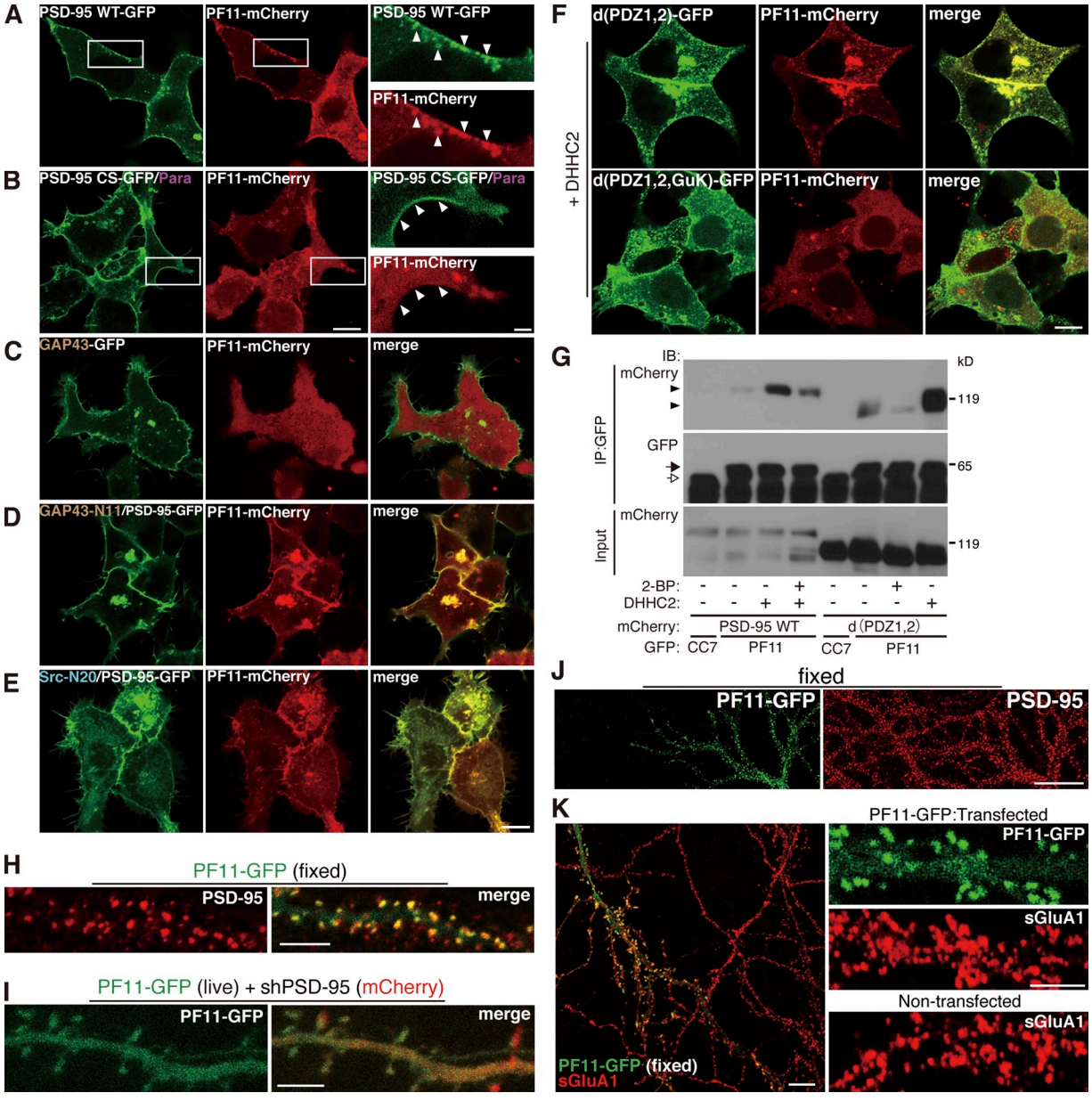

Figure S1. **PF11 as a conformation-specific intrabody to recognize palmitoylated PSD-95 in heterologous cells and neurons.** (A–E) Live imaging of HEK293T cells coexpressing PF11-mCherry and one of the PSD-95 chimeric constructs depicted in Fig. 3 F. (A) Wild-type PSD-95-GFP (palmitoylated by DHHC2) targeted to the plasma membrane (specific binding of PF11-mCherry, arrowheads); (B) PSD-95 CS-GFP/Para, in which the C-terminal palmitoylated motif of paralemmin was added to the C terminus of PSD-95 CS-GFP (no specific binding of PF11, arrowheads); (C) GAP43, an N-terminally palmitoylated protein (no specific binding); (D and E) GAP43-N11/PSD-95-GFP and Src-N20/PSD-95-GFP, in which the N-terminal palmitoylation motif of PSD-95 was replaced with that of GAP43 (11 aa) or with the myristoylation motif of Src (20 aa) (specific binding of PF11). Bars, 10 µm (B, magnified, 2 µm). (F) Both PSD-95 d(PDZ1,2)-GFP, which lacked the first and second PDZ domains, and PSD-95 d(PDZ1,2, GuK)-GFP, which further lacked the GuK domain, were targeted to the plasma membrane in the presence of DHHC2, but only PSD-95 d(PDZ1,2)-GFP was recognized by PF11. Bar, 10 µm. (G) PF11 binding is palmitoylation dependent. The indicated plasmids were cotransfected and PF11-GFP or CC7-GFP was immunoprecipitated (IP) by an anti-GFP antibody. Closed arrow, PF11-GFP; open arrow, CC7-GFP; closed arrowheads, coimmunoprecipitated PSD-95 and PSD-95 d(PDZ1,2). (H–K) PF11-GFP was expressed in hippocampal neurons and imaged in fixed (H, J, and K) or living (I) cells. (H) PF11-GFP puncta (green) overlapped with endogenous PSD-95 postsynaptic clusters (red). Bar, 5 µm. (I) Postsynaptic labeling of PF11-GFP is specifically attributed to endogenous PSD-95. PF11-GFP was transfected with shPSD-95 to knock down PSD-95 expression together with mCherry. PF11-GFP was diffusely distributed in the dendrites of shPSD-95 transfected neurons. Bar, 5 µm. (J) PF11-GFP expression does not affect endogenous PSD-95 clusters. Bar, 20 µm. (K) PF11-GFP expression does not affect the staining pattern of surface-expressed AMPARs (GluA1 subunit, red). Bars, 10 µm (magnified, 5 µm).

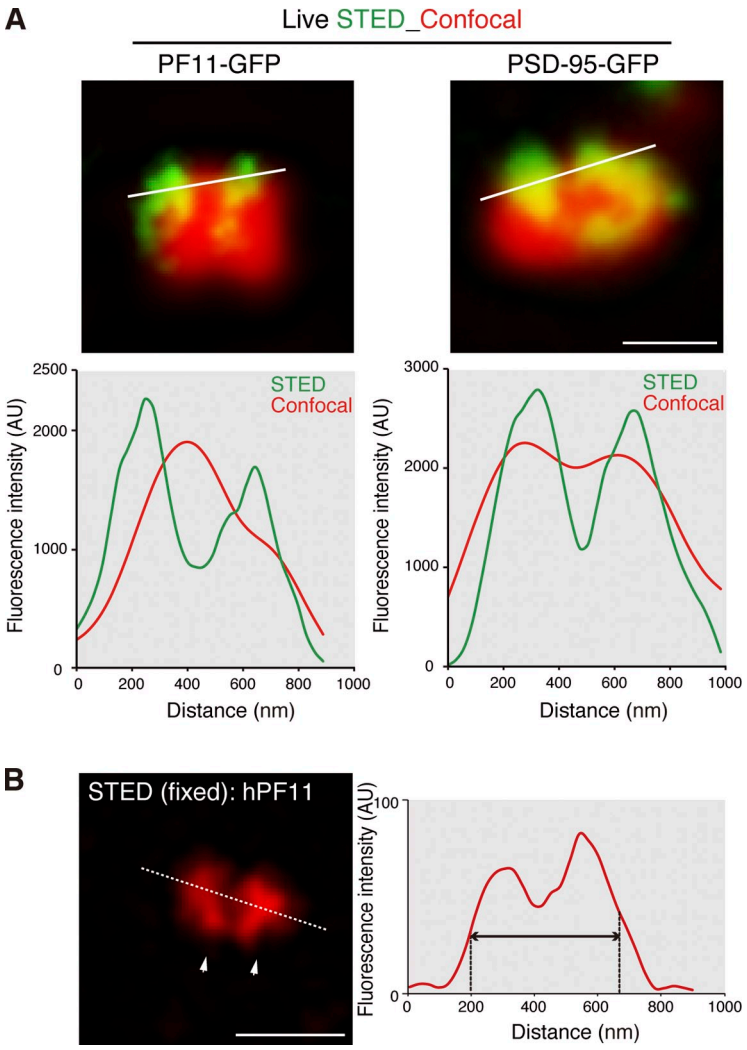

Figure S2. **Postsynaptic nanodomains visualized by PF11-GFP, PSD-95-GFP, and hPF11.** (A) Hippocampal neurons were nucleofected with PF11-GFP or PSD-95-GFP, and the same field of neurons was sequentially live-imaged in confocal (red pseudocolor) and STED (green) modes. Intensity profiles (bottom panels) were generated along the white lines in the top images. Individual nanodomains were distinguished by STED microscopy using both PF11-GFP and PSD-95-GFP, which were separated by narrow gaps (green lines). Under these conditions, the conventional confocal mode could not resolve nanodomains (red lines). Representative images and profiles from more than three repeats are shown. Bar, 500 nm. (B) The size of PF11-labeled postsynaptic membrane regions was measured to calculate a frequency histogram (see Fig. 4 G). Intensity profiles were generated along the longest axis of postsynaptic membrane regions visualized by STED imaging of hPF11-stained neurons, as depicted here for a representative image from Fig. 4 F. For example, fluorescence intensity was measured along the white dashed line of a postsynaptic membrane region with two nanodomains (left, arrowheads), and FWHM on the obtained intensity profile (right, red line) was calculated (horizontal black arrow, FWHM 480 nm). Vertical dashed lines are set at half maxima. A representative profile is shown (450 clusters from 6 neurons, 3 independent experiments). Bar, 500 nm.

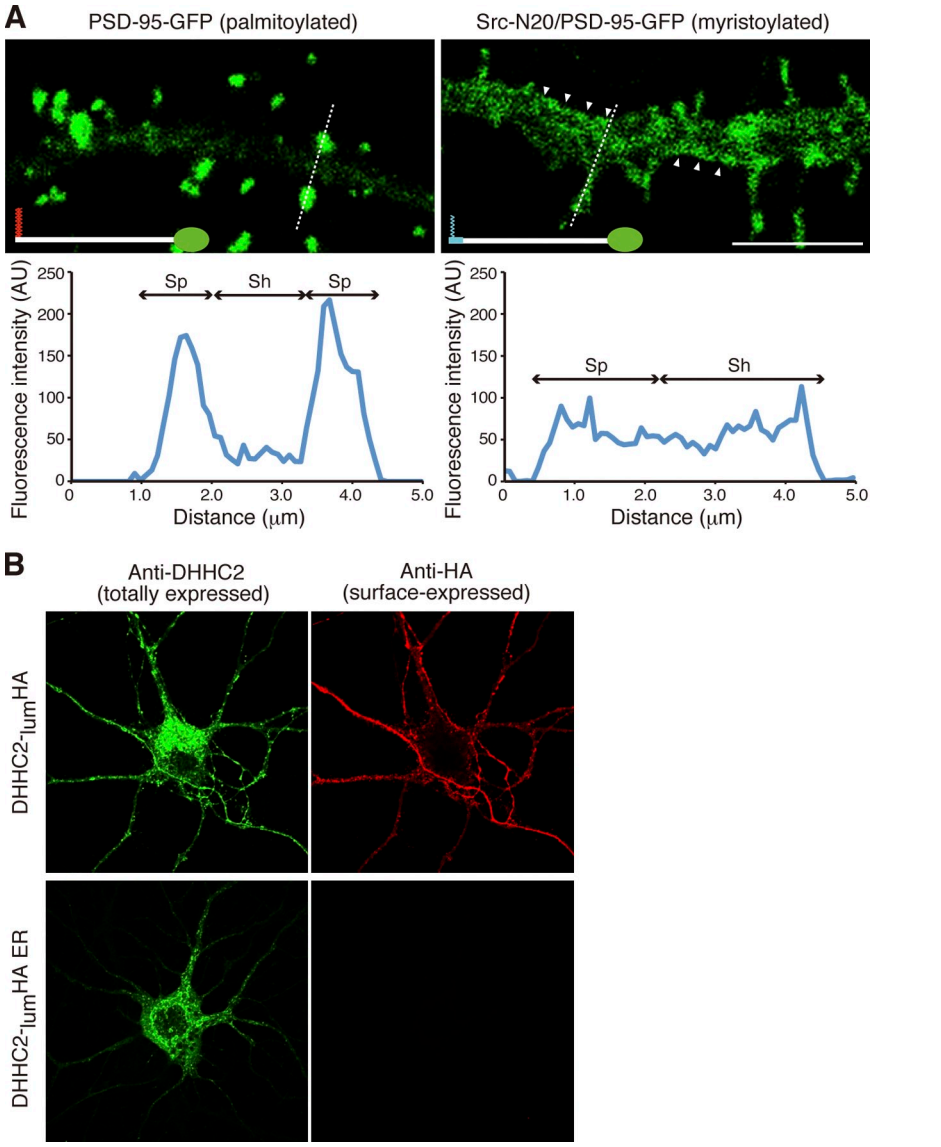

Figure S3. **Palmitoylation of PSD-95 is necessary for its postsynaptic clustering.** (A) Palmitoylation is a unique type of lipidation that mediates efficient postsynaptic clustering of PSD-95. Palmitoylated PSD-95-GFP or *N*-myristoylated PSD-95-GFP (Src-N20 in Fig. 3 F) was expressed in hippocampal neurons and live-imaged. Intensity profiles of the GFP fluorescence along the white dashed lines across dendritic shafts are shown (bottom panels). Arrowheads indicate GFP signals at the dendritic plasma membrane wrapping the dendritic shaft. Representative profiles from six repeats are shown. Sp, spine; Sh, dendritic shaft. Bar, 5 μm. (B) DHHC2-$_{lum}$HA ER, with an ER retention signal, EKKNR, remains at the ER and is not inserted into the plasma membrane. Surface-expressed DHHC2-HA was labeled by rat anti-HA (red) before cell permeabilization, and then total DHHC2-HA was stained by a mouse anti-DHHC2 antibody (green). Bar, 10 μm.

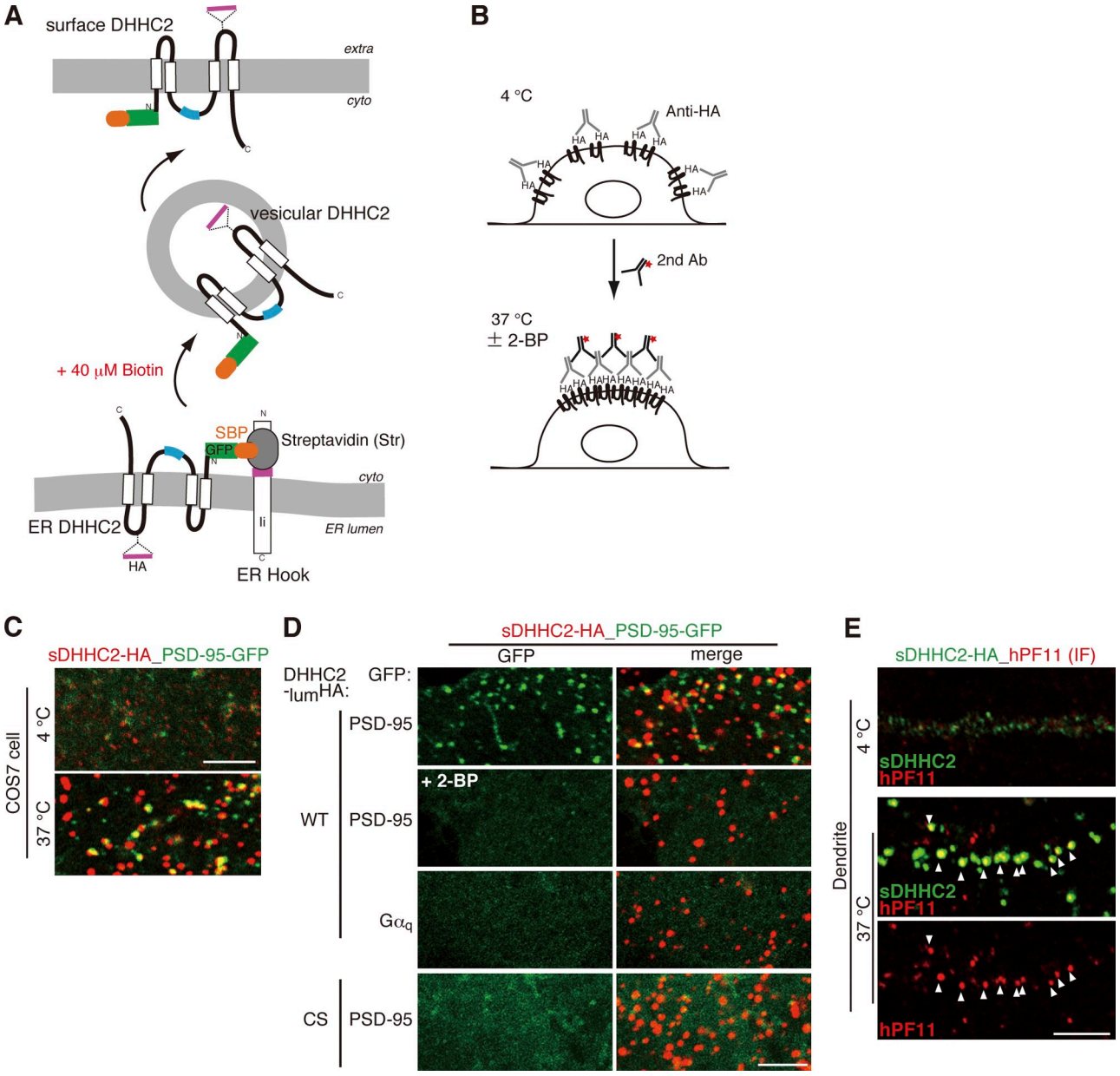

Figure S4. **Cell-surface DHHC2 generates PSD-95 clusters through its palmitoylating activity.** (A) Schematic diagram of RUSH assay (Fig. 7, A and B). Streptavidin-binding peptide (SBP)–fused GFP-DHHC2 (SBP-GFP-DHHC2) was hooked at the ER by interaction with the streptavidin (Str)-fused ER-resident protein Ii. Upon the addition of biotin, SBP-GFP-DHHC2 was released from the ER, entered the Golgi apparatus, and underwent vesicle trafficking to its final destination, the plasma membrane. After the addition of biotin, the trafficking of DHHC2-GFP and the cotransfected PSD-95-mCherry was time-lapse imaged. (B) Schematic diagram of forced engagement of DHHC2 on the cell surface. COS7 cells were transfected with DHHC2-$_{lum}$HA and the indicated GFP-fused proteins. Live cells were incubated with an anti-HA antibody at 4°C. After washing, the cells were treated with a Cy3-conjugated secondary antibody for 1 h at 4°C and then incubated for 1 h at 37°C to promote clustering of DHHC2-$_{lum}$HA on the plasma membrane. (C and D) After the engagement of surface-expressed DHHC2-$_{lum}$HA with anti-HA antibody at 37°C in COS7 cells, DHHC2-$_{lum}$HA and PSD-95- or Gα_q-GFP were visualized in red and green, respectively. Engagement of DHHC2 on the cell surface efficiently recruited PSD-95, but not Gα_q, another palmitoylated protein that is not a substrate of DHHC2. Recruitment of PSD-95 to the cell surface DHHC2 aggregates was completely blocked by incubation with 2-BP during DHHC2 engagement, which is indicative of the requirement for local and continuous palmitoylating activity. Cell surface engagement of inactive DHHC2 mutant CS-$_{lum}$HA did not induce PSD-95 recruitment. As a negative control of the engagement, cells were incubated at 4°C without shifting to 37°C (C, top). Bars, 5 µm. (E) Engagement of DHHC2-$_{lum}$HA (sDHHC2, green) in neurons induces clusters of endogenous palmitoylated PSD-95 (hPF11, red) at the dendritic membrane (arrowheads). Bar, 5 µm.

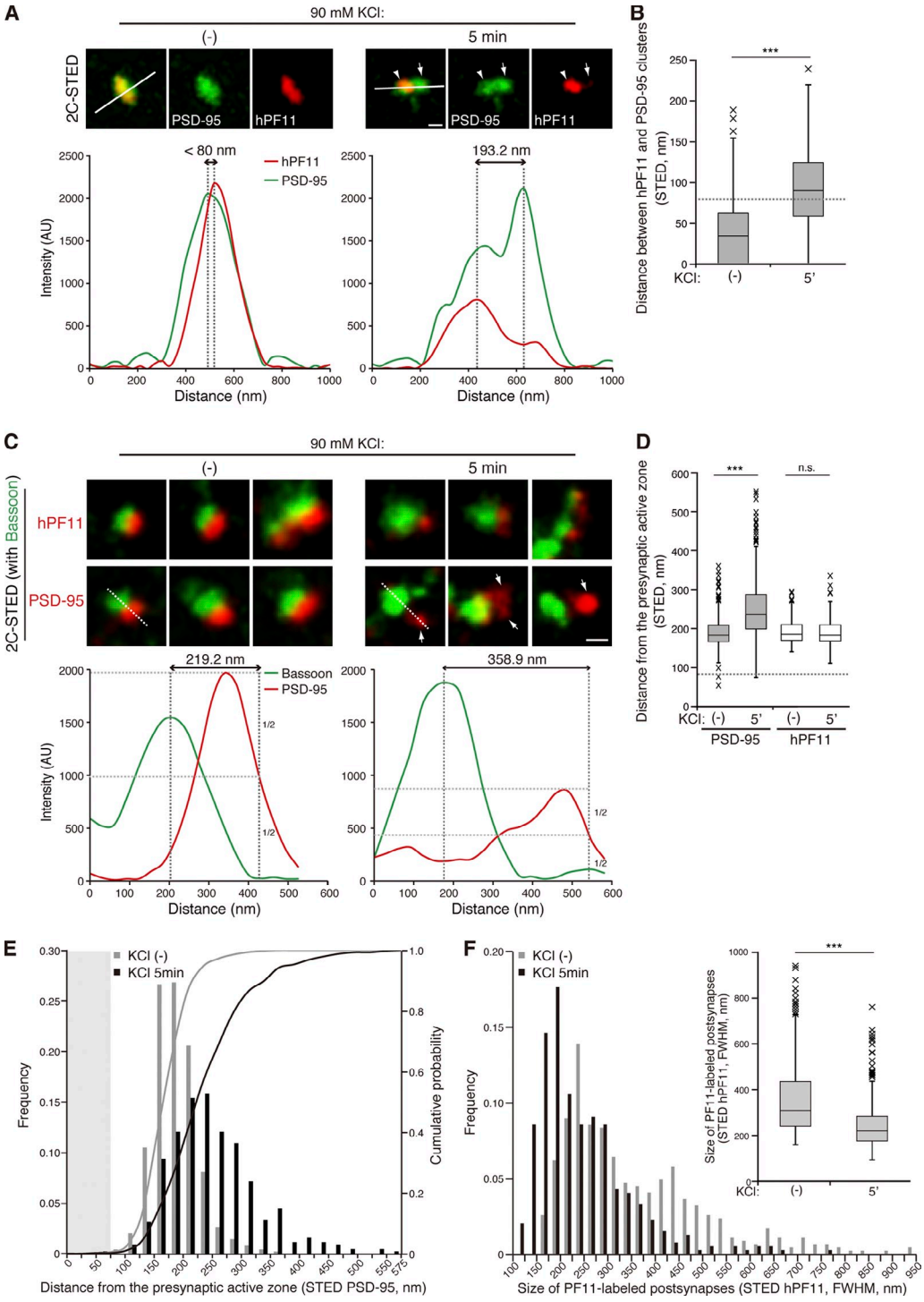

Figure S5. **Acute synaptic activation causes intra-spine delocalization of depalmitoylated PSD-95 and reduces the size of the postsynaptic membrane region.** (A and B) Upon depalmitoylation by enhanced synaptic activation (90 mM KCl, 5 min), PSD-95 dissociates from the postsynaptic membrane (Fig. 8, C and D). The distance between the peaks with the highest intensity for hPF11 (top panels, red) and PSD-95 antibody (green)-labeled clusters was measured on the intensity profile of 2C-STED imaging (bottom panels) along a white line (1 µm, in top). Arrowheads and arrows denote the positions of the strongest hPF11 and PSD-95 labeling, respectively. In total, 150–200 clusters from 10 neurons (two independent experiments) were analyzed (representative profiles are shown in A; Bar, 200 nm). A dashed line indicates the resolution limit of STED microscopy (80 nm, B). ***, $P < 0.001$ by Student's *t* test. (C–E) Dissociation of PSD-95 from the synaptic sites upon depolarization by high K^+. (C) Hippocampal neurons treated with 90 mM KCl for 5 min were stained by hPF11 (top panels, red) or anti-PSD-95 (bottom, red) with anti-bassoon (green) antibodies, and visualized by STED microscopy. The intensity profiles along white dashed lines are shown. To quantify the delocalization of PSD-95 from the synaptic sites, the distance between the peak position of bassoon labeling (green line) and the distant half maximum position of PSD-95 labeling (red line) was measured. Arrows, PSD-95 signals observed away from the synapse. Bar, 200 nm. (D and E) Quantification results are shown. In total, ~500 clusters from 10 neurons were analyzed. ***, $P < 0.001$ by Student's *t* test. Light gray region indicates the subresolution range for STED imaging (E). (F) The size of postsynaptic membrane regions is rapidly reduced upon depolarization by high K^+. The postsynaptic membrane labeled with hPF11 was visualized and measured as in Fig. S2 B. Results are shown in histograms and box-and-whisker plots. The size distribution obtained in the absence of KCl treatment is also shown in Fig. 4 G. In total, ~400 clusters from 5 neurons (two independent experiments) were analyzed. ***, $P < 0.001$ by Student's *t* test.

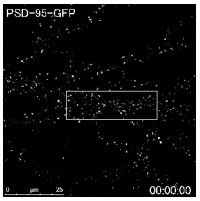

Video 1. **FRAP analysis of live neurons expressing PSD-95-GFP.** The dendritic region indicated by a white rectangle was bleached with a 488-nm laser. We acquired xyz stacks at a spacing of 0.5 µm (5–7 sections) every 2 min for 60 min with time-lapse confocal microscopy (TCS SP5 II; Leica). Each frame represents a maximal intensity projection. Even spines located at the edge of the bleached field showed a similarly slow recovery. The movie is representative of three independent experiments. Corresponding to Fig. 5 A.

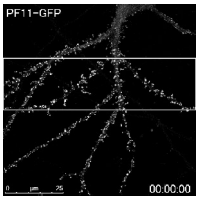

Video 2. **FRAP analysis of live neurons expressing PF11-GFP.** The dendritic region indicated by a white rectangle was bleached with a 488-nm laser. We acquired xyz stacks at a spacing of 0.5 µm (5–7 sections) every 2 min for 60 min with time-lapse confocal microscopy (TCS SP5 II; Leica). Each frame represents a maximal intensity projection. The movie is representative of three independent experiments. Corresponding to Fig. 5 A.

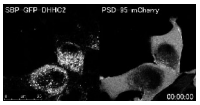

Video 3. **RUSH assay for GFP-DHHC2 WT.** HEK293T cells were transfected with a RUSH vector containing Ii-streptavidin as an ER-hook and SBP-GFP-DHHC2 as a reporter, along with pGW1-PSD-95-mCherry. After 20 h of expression, at time 00:00, release of SBP-GFP-DHHC2 was induced by the addition of biotin, and trafficking of SBP-GFP-DHHC2 (left) and PSD-95-mCherry (right) was monitored every 1 min for 90 min by time-lapse confocal microscopy (TCS SP5 II; Leica). Corresponding to Fig. 7 A.

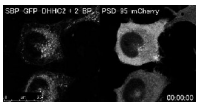

Video 4. **RUSH assay for GFP-DHHC2 WT in the presence of 2-BP.** HEK293T cells were transfected with a RUSH vector containing Ii-streptavidin as an ER-hook and SBP-GFP-DHHC2 as a reporter, along with pGW1-PSD-95-mCherry. After 20 h of expression, at time 00:00, release of SBP-GFP-DHHC2 was induced by the addition of biotin together with 2-BP (100 µM), an inhibitor of palmitoylation. The trafficking of SBP-GFP-DHHC2 (left) and PSD-95-mCherry (right) was monitored every 1 min for 90 min by time-lapse confocal microscopy (TCS SP5 II; Leica). Corresponding to Fig. 7 A.

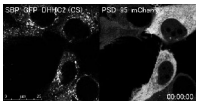

Video 5. **RUSH assay for catalytically inactive GFP-DHHC2 CS.** HEK293T cells were transfected with a RUSH vector containing Ii-streptavidin as an ER-hook and SBP-GFP-DHHC2 CS as a reporter, along with pGW1-PSD-95-mCherry. After 20 h of expression, at time 00:00, release of SBP-GFP-DHHC2 CS was induced by the addition of biotin and the trafficking of SBP-GFP-DHHC2 CS (left) and PSD-95-mCherry (right) was monitored every 1 min for 90 min by time-lapse confocal microscopy (TCS SP5 II; Leica). SBP-GFP-DHHC2 CS trafficking to the plasma membrane did not affect PSD-95 localization. Corresponding to Fig. 7 B.